Smart Ultrasound Device for Non-Invasive Real-Time Myocardial Stiffness Quantification of the Human Heart

Olivier Pedreira, Mafalda Correia, Simon Chatelin, Olivier Villemain, Guillaume Goudot, Stephane Thiebaut, Gioia Bassan, Emmanuel Messas, Mickael Tanter, Clement Papadacci, et al.

Smart Ultrasound for non-invasive real-time myocardial stiffness quantification of the human heart

Olivier Pedreira, Mafalda Correia, Simon Chatelin, Olivier Villemain, Guillaume Goudot, Stéphane Thiébaut, Gioia Bassan, Emmanuel Messas, Mickaël Tanter, Clément Papadacci*, and Mathieu Pernot*

Abstract—**Quantitative assessment of myocardial stiffness is crucial to understand and evaluate cardiac biomechanics and function. Despite the recent progresses of ultrasonic shear wave elastography, quantitative evaluation of myocardial stiffness still remains a challenge because of myocardium location, motion, large elasticity changes and strong elastic anisotropy. In this paper we introduce a smart ultrasound approach for non-invasive real-time quantification of shear wave velocity (SWV) and elastic fractional anisotropy (FA) in locally transverse isotropic elastic medium such as the myocardium. We demonstrated, that this approach can quantify accurately SWV in the range of 1.5 to 6 m/s in transverse isotropic medium (FA<0.7) using numerical simulations. The approach was experimentally validated on calibrated phantoms and anisotropic ex vivo tissues. A mean absolute error of 0.22 m/s was found when compared to gold standard measurements. Finally, in vivo feasibility of myocardial anisotropic stiffness assessment was evaluated in four healthy volunteers on the antero-septo basal segment and on anterior free wall of the right ventricule (RV) in end-diastole. A mean longitudinal SWV of 1.08 ± 0.20 m/s was measured on the RV and 1.74 ± 0.51 m/s on the Septum with a good intra-volunteer reproducibility (± 0.18 m/s). This approach has the potential to become a clinical tool for the quantitative evaluation of myocardial stiffness and diastolic function.**

***Index Terms*— Myocardial Stiffness, Shear Wave Velocity, Acoustic Radiation Force.**

Manuscript submitted XXX
This study was supported by the European Research Council under the Horizon 2020 Framework Program / ERC Grant Agreement n° 665113. This study was also supported by BPI FRANCE (PACIFIC project) and INSERM Transfert (COPOC project). We acknowledge the ART (Technological Research Accelerator) biomedical ultrasound program of INSERM.
O. Pedreira (pedreiraolivier@gmail.com), M. Correia (mafilipa.correia@gmail.com), S. Chatelin (simon.chatelin@gmail.com), O. Villemain (olivier.villemain@sickkids.ca), S. Thiébaut (stephanethiebaullt@gmail.com), G. Bassan (gioia.bassan@gmail.com), M. Tanter (mickael.tanter@gmail.com), C. Papadacci (clement.papadacci@espci.fr), and M. Pernot (mathieu.pernot@gmail.com) are with Physics for Medicine Paris, INSERM U1273, ESPCI Paris, PSL University, CNRS FRE 2031, Paris, France. *C. Papadacci and M. Pernot contributed equally to this study.
G. Goudot (guillaume.goudot@gmail.com) and E. Messas (emmanuel.messas@aphp.fr) are with Hôpital Européen Georges Pompidou, APHP, Vascular Medicine Department, Paris, France.

I. INTRODUCTION

Myocardial stiffness is a key biomechanical property of the cardiac mechanics and function. Myocardial stiffness alteration during contraction or relaxation is associated with heart failure, and consequently high risk of death[1]–[3]. Up to date, despite the urgent clinical need, there is no non-invasive method available in clinical practice to assess myocardial stiffness quantitatively [4].

The advent of ultrafast ultrasound imaging (UF) almost 20 years ago has enabled the observation of mechanical shear waves in soft tissues. Based on the intrinsic relationship between shear wave velocity (SWV) and the shear modulus of soft tissues [5], UF imaging was rapidly envisioned as a tool for non-invasive and quantitative imaging of soft tissues' elastic properties. The combination of UF imaging and the remote generation of shear waves through the acoustic radiation force enabled the so-called Shear Wave Elastography (SWE) modality which was successfully developed in the clinics for quantitative mapping of breast, liver and thyroid elasticity. Cardiac applications of SWE were also investigated extensively for the measurement of myocardial stiffness in the beating heart of preclinical models [6] [7] [8]. With this approach, shear wave velocity could be measured at any moment of the cardiac cycle to assess stiffness variation [9], to provide a contractility index [10] or passive property estimations [11] respectively based on systolic and diastolic elastic properties. More recently, SWE was translated to human applications and the clinical proof of concept of myocardial SWE was demonstrated on healthy volunteer [12], [13] and hypertrophic cardiomyopathy patients [14].

Nevertheless, an important issue remained unsolved: the dependence of shear velocity with the local orientation of myocardial fibers. Indeed, muscular, tendinous and myocardial tissues are composed of fibers locally oriented along a principal direction (longitudinal direction). These soft solids can be assumed as locally transverse isotropic materials [26], [27] in which a single shear modulus is no longer adequate to characterize the elastic properties. As stiffness (and SWV) is higher along fibers than across them [15], the complete stiffness tensor is required to characterize the elastic properties of anisotropic tissues such as the myocardium. Moreover, fiber orientation in the myocardium follows a complex helicoidal

distribution of bundle which is patient dependent. Therefore, with 2D imaging, shear wave velocity is measured in an unknown direction with respect to the fiber orientation creating important variability on SWV evaluation and a certain ambiguity to what stiffness parameter is really measured.

A potential solution to solve this problem is the Elastic Tensor Imaging (ETI) approach [18], [19] to retrieve the full wave propagation from several measurements performed at different angles using a mechanical rotation of the probe, but this setup was not applicable in real-time and thus not suitable for clinical use. More recently, ETI was implemented using 3D UF with matrix probes which offered the possibility to track the transient shear wave in a single 3D acquisition [20][21]. However, this approach relies on complex and costly hardware in terms of probes, wirings and electronics to drive thousands of independent piezoelectric elements, and cannot be applied in its current form to clinical applications.

In this work, we propose an innovative solution based on a smart ultrasound approach to achieve real-time myocardial anisotropic stiffness quantification in human patients. The transducer was designed specifically for imaging fibrous tissues and to retrieve the SWV parameters in locally transverse isotropic medium. The concept was validated using numerical simulations in the first part of the study. Then, the device was experimentally validated against gold standard in calibrated phantoms and ex vivo fibrous tissues. Finally, in vivo and transthoracic feasibility of end-diastolic myocardial stiffness evaluation was demonstrated in human volunteers. This approach has the potential to become a clinical tool for the quantitative evaluation of myocardial stiffness in diastole but also at any time of the cardiac cycle.

II. MATERIALS AND METHODS

A. Shear Wave Velocity in transverse anisotropic medium

Let's consider a linear transverse isotropic elastic solid with a (y_0, x_0) isotropic plane (i.e. the plane normal to the fiber direction) and z_0 axis of symmetry (Figure 1). The fourth-rank stiffness tensor can be simplified by using the 2-index Voigt notation:

$$C = \begin{bmatrix} c_{11} & c_{11}-2c_{66} & c_{13} & 0 & 0 & 0 \\ c_{11}-2c_{66} & c_{11} & c_{13} & 0 & 0 & 0 \\ c_{13} & c_{13} & c_{33} & 0 & 0 & 0 \\ 0 & 0 & 0 & c_{44} & 0 & 0 \\ 0 & 0 & 0 & 0 & c_{44} & 0 \\ 0 & 0 & 0 & 0 & 0 & c_{66} \end{bmatrix} \quad (1)$$

$$\text{where } c_{13} = \sqrt{c_{33}(c_{11}-c_{66})}$$

The Christoffel equation was used to derive the velocity of mechanical waves that propagate in such solid. The group velocity of a shear wave polarized along x_1 and propagating in the (y_1, z_1) plane (probe coordinate system) can be expressed as follow [22]:

$$\rho v_r(\theta)^2 = \frac{C_{44}C_{66}}{C_{44}sin^2(\theta+\theta_0)+C_{66}cos^2(\theta+\theta_0)} \quad (2)$$

With $v_r(\theta)$ the group velocity, θ the angle defining the propagation direction and θ_0 the orientation of the fibers in the (y_1, z_1) probe coordinate system.

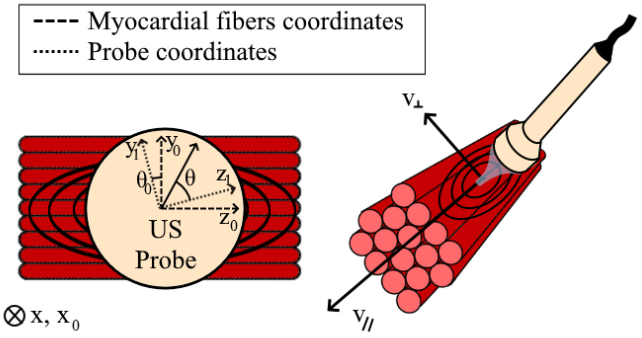

Fig. 1 Representation of fibers orientation in the probe coordinate system (y_1, z_1). Fibers are oriented along θ_0 . The SW is tracked along a direction θ. Representation of parallel SWV ($v_{\parallel}$) direction and perpendicular SWV ($v_{\perp}$) direction.

B. Deriving SWV using Elastic Tensor Imaging (ETI)

The concept of ETI was introduced by Lee et al. [19]. Shear wave propagation properties (c_{44}, c_{66}, θ_0) were retrieved from a limited number of shear wave velocity measurements (v_{rN}) estimated along different propagation directions (θ_N). Linearization of Eq.2 was performed:

$$\frac{1}{\rho {v_r}^2} = \frac{1}{2\,C_{44}C_{66}}.\begin{pmatrix} C_{44}(1-\cos(2(\theta+\theta_0))) \\ +\,C_{66}\,(1+\cos(2(\theta+\theta_0))) \end{pmatrix} \quad (3)$$

Then

$$\frac{2}{\rho {v_r}^2} = \frac{C_{44}+C_{66}}{C_{44}C_{66}} + \frac{C_{66}-C_{44}}{C_{44}C_{66}}\cos(2\theta)\cos(2\theta_0) - \frac{C_{66}-C_{44}}{C_{44}C_{66}}\sin(2\theta)\sin(2\theta_0) \quad (4)$$

A change of variables is performed to simplify the notations:

$$\begin{bmatrix} X_1 \\ X_2 \\ X_3 \end{bmatrix} = \begin{bmatrix} (C_{44}+C_{66})\,/\,C_{44}C_{66} \\ ((\,C_{66}-C_{44})\,/\,C_{44}C_{66}\,)*\cos(2\theta) \\ ((\,C_{44}-C_{66})\,/\,C_{44}C_{66}\,)*\sin(2\theta) \end{bmatrix} \quad (5)$$

We obtain a system of linear equations composed of the different measurements v_{rN} performed along different directions θ_N:

$$\begin{bmatrix} 2/\rho {v_{r1}}^2 \\ \vdots \\ 2/\rho {v_{rN}}^2 \end{bmatrix} = \begin{bmatrix} 1 & \cos(2\theta_1) & \sin(2\theta_1) \\ \vdots & \vdots & \vdots \\ 1 & \cos(2\theta_N) & \sin(2\theta_N) \end{bmatrix}.\begin{bmatrix} X_1 \\ X_2 \\ X_3 \end{bmatrix} = \phi.\begin{bmatrix} X_1 \\ X_2 \\ X_3 \end{bmatrix} \quad (6)$$

Inversion of the linear system can be performed with at least three independent measurements using the least-square method to provide an estimate of X_1, X_2, X_3

$$\begin{bmatrix} X_1 \\ X_2 \\ X_3 \end{bmatrix} = (\phi^T.\phi)^{-1}.\phi^T.\begin{bmatrix} 2/\rho {v_{r1}}^2 \\ \vdots \\ 2/\rho {v_{rN}}^2 \end{bmatrix} \quad (7)$$

Finally, we obtain the three unknown parameters as follow:

$$\theta_0 = \frac{1}{2}\text{atan}\left(\frac{X_3}{X_2}\right)$$

$$C_{66} = \frac{1}{2\left(X_1 - \frac{X_2}{\cos(2\theta_0)}\right)} \text{ and } C_{44} = \frac{1}{2\left(X_1 + \frac{X_2}{\cos(2\theta_0)}\right)} \quad (8)$$

Consequently, the shear modulus along and across the fibers and the fiber direction can be derived using at least 3 arbitrary measurements of the wave propagation in independent directions. Herein, we designed a dedicated probe based on this principle. In the following, the medium properties will be expressed in term of shear velocity along (parallel $v_{\parallel}$) and across (perpendicular $v_{\perp}$) the fibers using the relationship:

$$v_{\parallel} = \sqrt{C_{66}/\rho}, \qquad v_{\perp} = \sqrt{C_{44}/\rho} \ , \tag{9}$$

We will also quantify the Fractional Anisotropy (FA) parameter, between 0 to 1 (Isotropic to infinite anisotropy) using the following expression:

$$FA = \sqrt{2}\,\frac{\sqrt{(v_{\perp} - v_m)^2 + (v_{\parallel} - v_m)^2}}{\sqrt{v_{\perp}{}^2 + v_{\parallel}{}^2}} \tag{10}$$

With v_m the mean velocity of perpendicular and parallel SWV.

C. Basic Principles

We designed an ultrasonic transducer composed of a small number of individual piezoelectric elements to generate remotely a shear wave using the acoustic radiation force and to detect the tridimensional shear wave propagation along different directions.

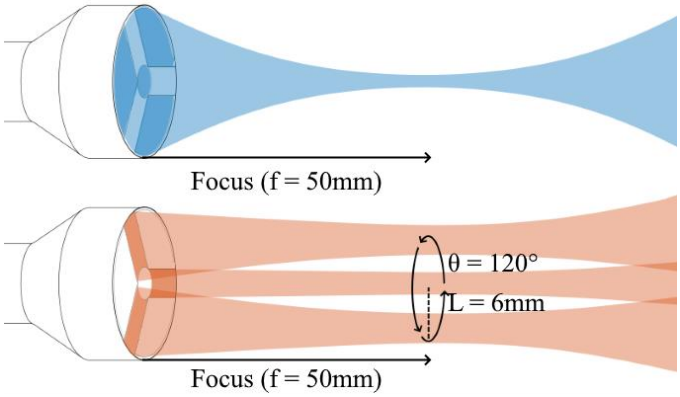

Fig. 2. Design of the ultrasound probe for multidirectional SWV assessment. In blue, representation of the pressure field generated by the five annular elements focused at f=50mm. In orange, representation of the pressure field generated by the three lateral elements. The lateral element centers are set radially with a 120° angular spacing.

The transducer was designed with five portions of concentric annular elements and three lateral elements (See figure 2). The annular elements are designed to 1) focus an ultrasound wave and generate the acoustic radiation force at the desired depth and 2) perform a real-time M-mode imaging for the positioning of the device. Lateral elements are set radially with a 120º angular spacing and are designed to estimate local tissue motion in dedicated locations surrounding the pushing location. The design of the probe is shown on Fig. 2. The two operation modes are presented: the focused mode for M-mode imaging and push generation and the pulse echo detection mode using the lateral elements (figure 2).

D. Numerical Simulation

In order to validate and understand the limitations of this approach, we performed in this section a four-steps numerical simulation that include both the acoustic and elastic wave propagations:

1. Acoustic radiation force field was computed in 3D with the ultrasound simulation software Field II.
2. Shear wave propagation generated by the acoustic radiation force in a transverse isotropic medium was computed using an anisotropic Green's function formalism.
3. Acoustic simulation was performed with Field II to compute the pulse echo signals received by the lateral elements during the propagation of the shear wave in a random scatterers' distributions. The scatterers' motion was set accordingly to the shear wave displacement field computed in step 2.
4. Axial tissue velocity was estimated from the pulse echo signals. Time of flight was estimated for each of the 3 lateral directions. Eq.7 was used to derive the medium properties (shear velocity along and across the fibers, fiber direction).

1) Simulation of the acoustic radiation force field

Field II ultrasound simulation software [23], [24] was used to compute the pressure field emitted by the concentric annular elements of the transducer over a 3D volume. The simulation parameters are detailed in Table 1. The acoustic radiation force field was obtained as $F = (2\alpha I)/c$ where I is the acoustic intensity computed as I= $P^2/(2Z)$ with P is the pressure amplitude and Z the acoustic impedance.

TABLE I
FIELD II - SIMULATION PARAMETERS (ACOUSTIC RADIATION FORCE)

Transducer discretization pitch	0.25 mm^2
Attenuation	150 dB/m
Transducer Center Frequency	2.5 MHz
Sampling Frequency	250 MHz
Transmit Duration	300 µs
Focus Depth	50 mm
Acoustic Impedance	1.48 x 10^6 $kg.m^{-1}.s^{-2}$
Simulation Grid	
- X Direction	-20 : 0.1 : 20 mm
- Y Direction	-20 : 0.1 : 20 mm
- Z Direction	0 : 0.1 : 150 mm

2) Simulation of the shear wave propagation

The shear wave propagation was computed using a transverse isotropic viscoelastic Green's function formalism [25]. In brief, this Green's function offers an analytical description of elastic wave propagation from a point source in a transverse isotropic material. Further details on the numerical method and implementation in soft tissues can be found in [26]. The acoustic radiation force 3D field computed in step 1 was used as the shear source term of the simulation. The displacement field **D**(x,y,z,t) created by the shear wave was computed at each temporal sampling point. We investigated a wide range of elastic parameters to assess the accuracy and the limitations of the method by varying the parallel and perpendicular shear velocities and the fractional anisotropy. In a first dataset, we computed seven configurations with a fixed FA of 0.2. The SWV, $v_{\parallel}$ was increased from 1.50 m/s to 6.00 m/s. For the second dataset, anisotropy was increased (FA from 0.2 to 0.78) while maintaining $v_{\perp}$ constant (1.5 m/s). The parameters of the simulation are summarized in Table II.

TABLE II
GREEN SIMULATION PARAMETERS

Compression Velocity	c_P	1500 m/s
Medium Density	ρ	1038 g/cm^3
Sampling Frequency	F_s	10 000 Hz
- 1st Dataset		
Perpendicular Shear Wave Velocity	$v_\perp$	[1.50 - 2.00 - 2.50 - 3.00 - 3.50 - 4.00 - 4.50] m/s
Parallel Shear Wave Velocity	$v_\parallel$	[2.00 - 2.67 - 3.33 - 4.00 - 4.67 - 5.33 - 6.00] m/s
- 2nd Dataset		
Perpendicular Shear Wave Velocity	$v_\perp$	[1.50 - 1.50 - 1.50 - 1.50 - 1.50 - 1.50 - 1.50] m/s
Parallel Shear Wave Velocity	$v_\parallel$	[2.00 - 2.50 - 3.00 - 3.50 - 4.00 - 4.50 - 5.00] m/s

3) Pulse-echo simulation of the shear wave detection

Pulse echo signals received by each of the 3 lateral elements were simulated using Field II. A collection of 20 000 randomly distributed scatterers was used to generate the backscattered signal. The displacement field $\boldsymbol{D(x,y,z,t)}$ obtained in the previous step was applied on the scatterers position $\boldsymbol{S_t = S_0 + D(x,y,z,t)}$. A pulse echo simulation was performed for each distribution $\boldsymbol{S_t}$ of the scatterers at high repetition rate (10000Hz). The set of radio-frequency signals was then generated for each lateral element and a uniform random noise equivalent to 5% of the maximum RF value was added.

4) Post-processing steps and shear velocity quantification

Axial tissue velocities were obtained at each depth and for each lateral element from successive RF signals using the Kasai estimator [27]. After low pass filtering (Butterworth filter, cut frequency 500Hz, order 5), the time of flight of the shear wave propagation was determined as the time to peak velocity [28] for each of the lateral element. The three parameters θ, C_{66} and C_{44} are derived from equation (7). Using eq.9, shear velocities along and across the fibers and the fiber directions were assessed. The result was displayed as an elliptical profile of the shear velocity. It should be noted that the velocity profile of equation (2) is not a pure ellipse [29] however for the sake of simplicity we will refer in the following as an "elliptic profile". A motion correction was applied to remove the overall motion of the tissue by subtracting the mean displacement within the duration of the UF acquisition. This step was necessary only for in vivo acquisitions on human heart.

E. Experimental validation

The probe presented in Section II.B was manufactured and connected to a research electronics (Vantage 64, Verasonics, Seattle, USA). A user interface software was developed to position the probe and trig the acquisitions.

1) M-Mode imaging

Harmonic M-Mode imaging was performed by using the concentric annular elements. Ultrasonic beams (central frequency of 2.1 MHz) were focused at a depth of 55 mm with a PRF of 480 Hz using a pulse inversion scheme. Backscattered signals were received, filtered and beamformed using a conventional delay and sum algorithm. A dedicated software was developed to provide a real time M-Mode imaging using the annular elements with an effective Framerate of 200 Hz to allow the positioning.

2) SWE sequence

To generate the SW a US burst at the frequency of 2.5 MHz was focused during 350µs. The push was immediately followed by UF acquisition using the three lateral elements. Pulse echo imaging was performed at high framerate (10 000 kHz) during 15ms. The signals received by the three laterals elements were then post processed. The post-processing method detailed in D.4 for synthetic data was applied to the experimental RF signals.

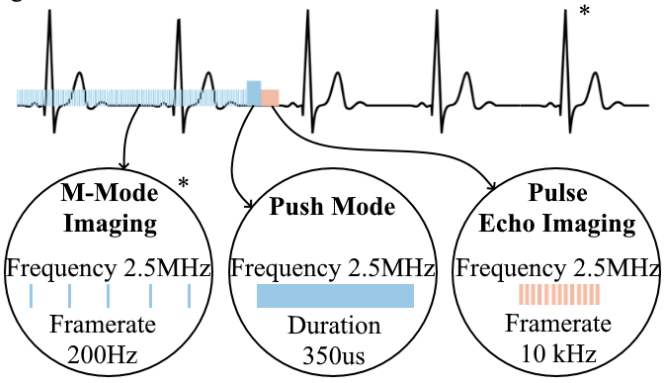

Fig. 3. Representation of the sequence for In-vivo stiffness evaluation. The device allows a live M-Mode imaging to correctly place the probe. Shear wave generation is performed in diastole using ECG trigger. Immediately following the push, the system switch to Pulse Echo Imaging with the lateral elements to track the shear wave. *ECG trigger and M-Mode Imaging are only used for in-vivo cardiac measurement.

3) Acoustic calibrations

The pressure field emitted by the annular and lateral elements were calibrated using a bilaminar PVDF membrane hydrophone (Acertara 805). The hydrophone was mounted on a 3-axis motorized Acertara measurement tank in order to scan the pressure field in the entire volume. The Mechanical Index (MI) and ISPTA were measured for the push beam and the lateral elements beams. The MI was 1.33 and TI was 0.87.

4) In Vitro Isotropic phantoms

Validation was performed on four isotropic calibrated phantoms (CIRS, Zerdine®, model 039) with SWV values of 0.92m/s – 1.49m/s – 2.58m/s and 3.49 m/s provided by the manufacturer. For each phantom, 100 measurements at different locations were done to evaluate the measurements variability.

5) Ex-Vivo tissue samples

Three ex-vivo samples of anisotropic skeletal muscles and left ventricular tissues were used. The first model was an ex-vivo bovine muscle sample, the second was a chicken breast and the last model was a porcine left ventricular sample. The samples were put in saline water and were imaged at a distance of Z = 50mm. A validation against shear wave speed measurements from Aixplorer® scanner (Supersonic Imagine, France), gold standard for SWE, was performed for the skeletal muscle samples using a linear conventional probe SL10-2 attached to a motorized rotation device.

6) Human acquisitions

Transthoracic acquisitions were performed on four healthy volunteers by a trained cardiologist. The volunteers were positioned in left lateral decubitus position. The probe was positioned in parasternal view and aligned on the antero septo basal segment using M-Mode imaging. The acquisition was triggered in mid diastole using the ECG and adjusted manually by the operator on the user interface. The sequence is represented in Figure 3. Five acquisitions were performed by the same operator on each volunteer at different heart beat to investigate the intra-volunteer reproducibility.

III. RESULTS

A. Numerical validation

The acoustic intensity map (spatial peak pulse average intensity map ISPPA) computed by Field II is shown on Figure 4. The maximum intensity was found at a depth of 57.5 mm. The -6dB focal spot dimensions was 61.1 mm in the axial direction and 1.4 mm in the radial direction.

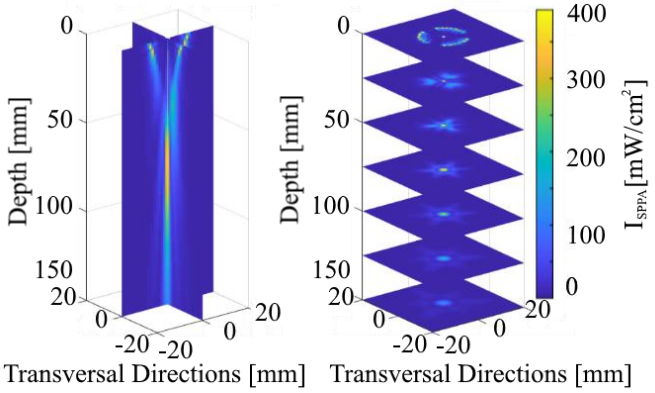

Fig. 4. Numerical Simulation of the push field and the shear wave generated. Acoustic intensity field of the annular elements computed with Field II, the probe is positioned at (0, 0, 0), top of the image.

The shear wave generated by the acoustic radiation force term was then computed using the Green's function formalism in transverse isotropic medium. An example of the resulting elliptic displacement wave front is shown on Figure 5.A at t=3.5ms for parallel and perpendicular shear wave speeds set respectively to 2.00 m/s and 1.50 m/s. Pulse-echo imaging was then simulated for each lateral element. The central positions of the lateral elements are superimposed on figure 5.A. After motion estimation, the temporal tissue velocity profile was obtained for the three lateral elements (Figure 5.B).

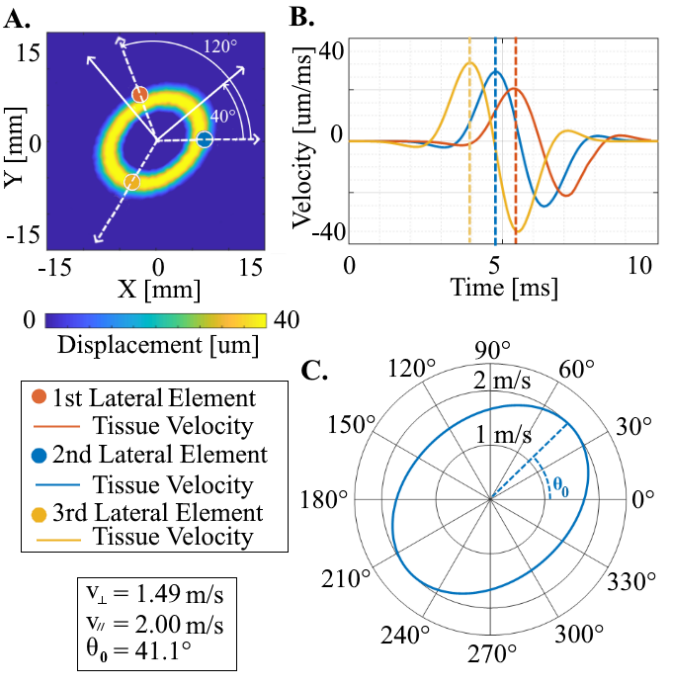

Fig. 5. **A.** Displacement field of the shear wave propagation at a depth of Z = 50mm and t = 3.5ms. The markers show the central position of the lateral elements. **B.** Tissue velocity estimated by the three lateral elements used to evaluate the shear wave speed. **C.** Medium properties were derived $v_{\parallel} =$ 2.00 m/s, $v_{\perp} = 1.49$ m/s and θ_0=41.1°, and the elliptic profile of the shear velocity was reconstructed.

Time of flight estimation was performed to assess the group velocity in the three directions. Finally, after inversion of Eq. 6, the shear modulus in parallel and perpendicular directions as well as the fiber direction were retrieved. The shear velocity profile shown in Figure 5.C was reconstructed from Eq.2. In this example, we obtained $v_{\parallel} = 2.00$ m/s, $v_{\perp} = 1.49$ m/s and θ= 41.1° which was in good agreement with the simulation parameters ($v_{\parallel} = 2.00$ m/s, $v_{\perp} = 1.50$ m/s and θ= 40.0°).

Results of the SWV computed by the simulation are presented on figures 6 and 7. Figure 6 presents the results for a fixed FA models. SWV estimates were in good agreement with the simulation parameters. The mean difference between the estimates and the theoretical parallel and perpendicular SWV was 0.11 m/s. The FA estimates were also close to the theoretical values with a mean absolute error of 0.078. Figure 7 show the results for the increased FA models. A good agreement was found between the SWV estimates and the simulation parameters with a mean difference between measured and theoretical values of 0.36 m/s and 0.065 between Theoretical and computed FA.

It should be noted that in both results, the estimation was particularly accurate for SWV below 5 m/s and becomes less accurate at higher velocity.

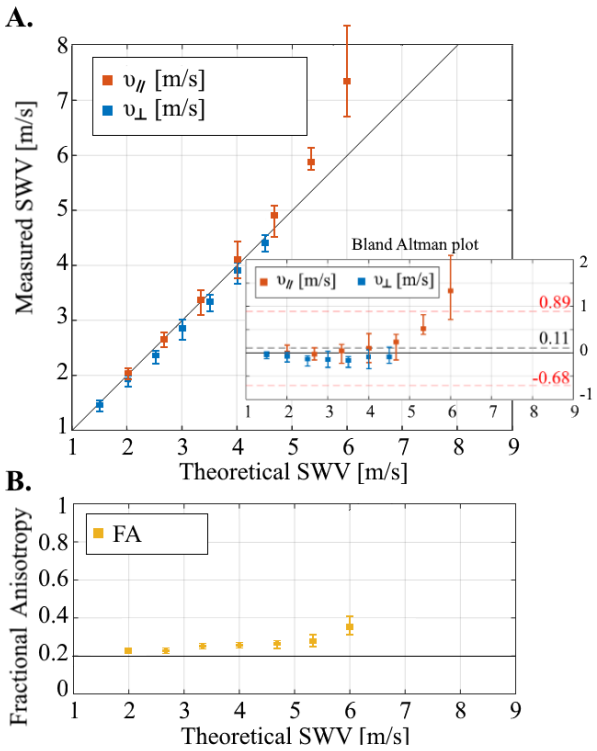

Fig. 6. Estimation of SWV (fixed FA). **A.** Estimated Shear Wave Velocity along parallel ($\upsilon_{\parallel}$) and perpendicular ($\upsilon_{\perp}$) direction. **B.** Bland Altman plot between measured and Theoretical SWV, mean value 0.11m/s, mean+0.96SD = 0.89m/s, mean-0.96SD = -0.68m/s **C.** Fractional anisotropy estimates, mean 0.26

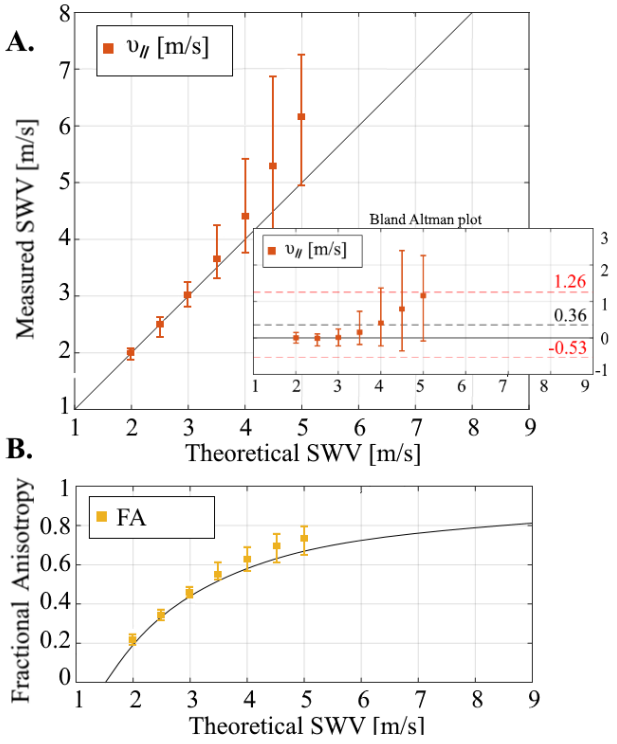

Fig. 7. Estimation of SWV (varying FA). **A**. Estimated Shear Wave Velocity along parallel ($\upsilon_{\parallel}$), perpendicular ($\upsilon_{\perp}$) direction. $\upsilon_{\perp}$ was fixed to 1.5 m/s. **B.** Bland Altman plot between measured and Theoretical SWV, mean value 0.36m/s, mean+0.96SD = 1.26 m/s, mean-0.96SD = -0.53 m/s **C.** Comparison of Fractional anisotropy estimates and theoretical values.

B. Experimental validation

1) Isotropic Phantoms

Shear wave velocity was evaluated in different calibrated phantoms. Agreement with the shear wave values provided by the manufacturer were found to be good (Figure 8) with a mean absolute error of 0.04 m/s.

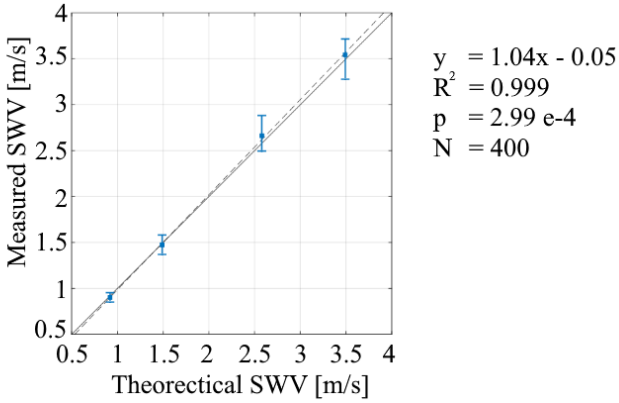

Fig. 8. Comparison of theoretical and measured shear wave velocity on 4 calibrated elastography phantoms. Measurement was repeated 100 times for each phantom.

2) Ex Vivo samples

The system was validated on two ex vivo skeletal muscles samples. In contrast with phantoms, the muscle samples were anisotropic and the elastic properties unknown. Tissue properties, were characterized using a 2D commercial shear wave elastography system (Aixplorer®) as explained in the methods section.

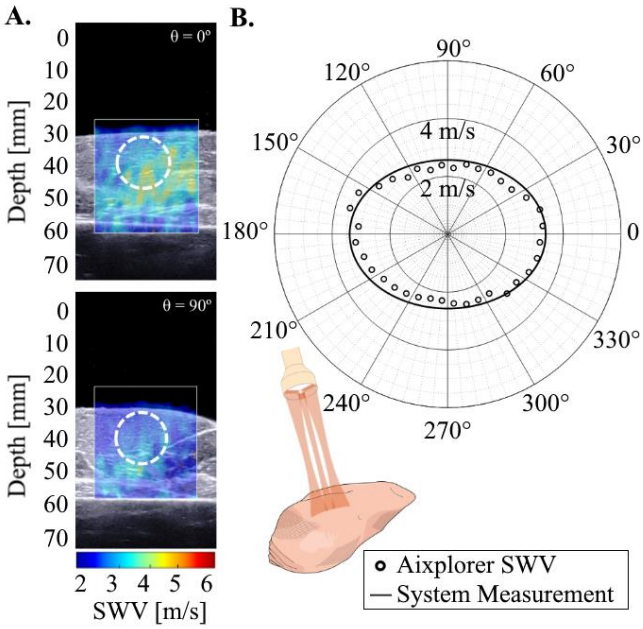

Fig. 9. In vitro validation in chicken breast. **A.** Shear modulus maps obtained using the Aixplorer® ultrafast scanner. The probe was turned each 10º to provide a stiffness estimate in each direction. Maps along (0º) and across (90º) the tissue fibers are shown. **B.** SWV profile reconstructed from a single acquisition using our smart sensor in solid line superimposed onto the Aixplorer® measurements each 10º.

Figure 9 shows the comparison of Aixplorer® ultrafast scanner measurements (with rotation of the probe) and the shear

velocity profile reconstructed with our system (without probe rotation) on chicken breast. It shows a good agreement of the measurements. A mean absolute error of 0.24 m/s was found. Table IV shows the transverse and longitudinal SWV estimates for the two measurements. With the clinical Aixplorer® Device SWV we measured $v_{\perp}$ = 2.3 m/s and $v_{\parallel}$ = 3.5 m/s versus $v_{\perp}$ = 2.57 m/s and $v_{\parallel}$ = 3.39 m/s

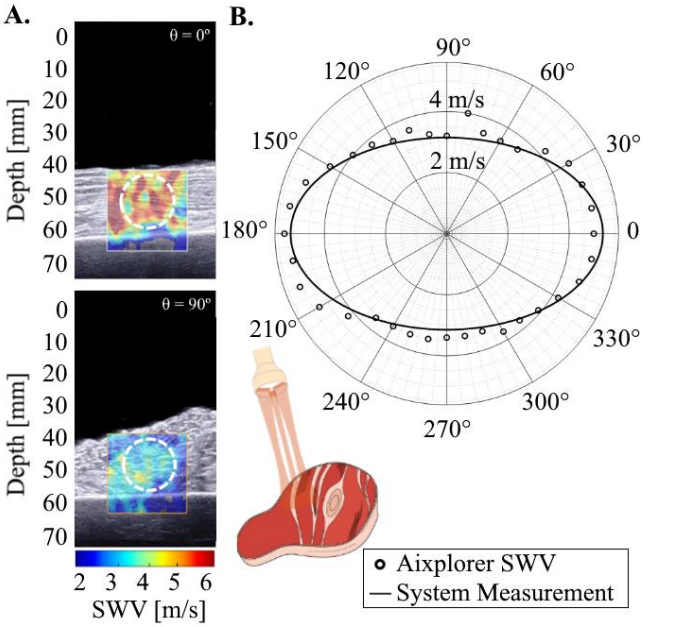

Fig. 10. In vitro validation in beef muscle. **A.** Shear modulus maps obtained using the Aixplorer®. The probe was turned each 10º to provide a stiffness estimate in each direction. Results along (0º) and across (90º) the tissue fibers are shown. **B.** SWV profile reconstructed from a single acquisition from the smart sensor in solid line superimposed onto the Aixplorer® measurements each 10º.

Figure 10 shows the same comparison on beef skeletal muscle. A good agreement was also found, the mean absolute error was 0.20 m/s which corresponded to a relative error of 4.88%. With the clinical Aixplorer® Device SWV we measured $v_{\perp}$ = 3.2 m/s and $v_{\parallel}$ = 5.3 m/s versus $v_{\perp}$ = 3.14 m/s and $v_{\parallel}$ = 5.10 m/s. Summary of the results is presented on table IV.

TABLE IV
FIELD II – EX VIVO RESULTS

Chicken Breast Tissue			
	Aixplorer® System		**Smart ultrasound device**
$v_{\perp}$	2.35 m/s	$v_{\perp}$	2.57 m/s
$v_{\parallel}$	3.25 m/s	$v_{\parallel}$	3.39 m/s
FA	0.22	**FA**	0.19
Beef Skeletal Muscle			
	Aixplorer® System		**Smart ultrasound device**
$v_{\perp}$	3.30 m/s	$v_{\perp}$	3.14 m/s
$v_{\parallel}$	5.05 m/s	$v_{\parallel}$	5.10 m/s
FA	0.29	**FA**	0.33

A last ex vivo experiment was performed in a fresh porcine left ventricular sample. Because the fibers directions vary rapidly across the wall it was not possible to compare directly with Aixplorer® measurements. Nevertheless, the variation of the shear velocity profiles with the smart ultrasound approach was analyzed across the wall. Figure 11 shows the reconstructed elliptic shear velocity profiles from Epicardium to Endocardium resulting in an approximately 90° rotation in fibers disposition in explanted ex vivo porcine LV measurement.

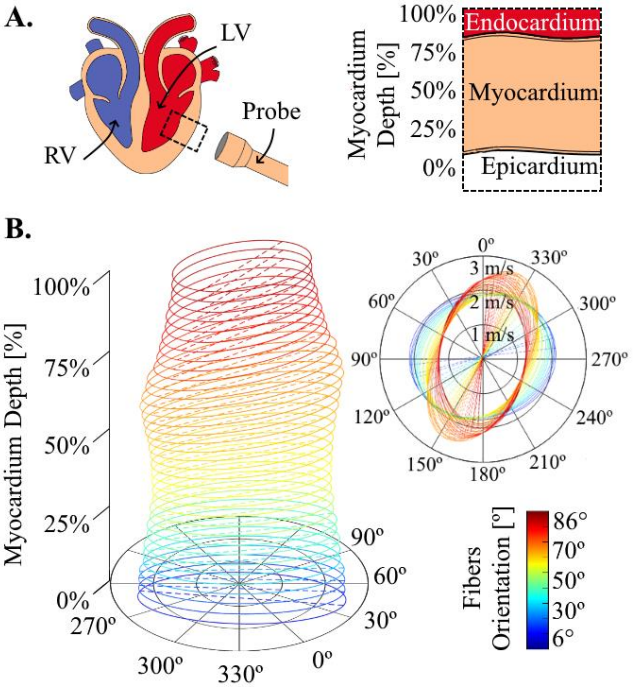

Fig. 11. Transmural variation of fibers orientation in ex vivo porcine samples. **A.** Schematic view of acquisition process, the US probe is aligned with the LV wall. **B.** Elliptic SWV profiles showing the fiber orientation as a function of transmural depth.

C. In Vivo feasibility

Finally, myocardial SWV was assessed in the heart of four human volunteers. Figure 12 shows an example of measurement. Real-time M-Mode positioning allowed visualization of RV and septal walls (Figure 12 A). Real-time ECG analysis allowed triggering acquisition in mid-diastole. SWV profiles in the RV and the septum of one volunteer is displayed on figure 12 B. RV was found softer and less anisotropic than the septum.

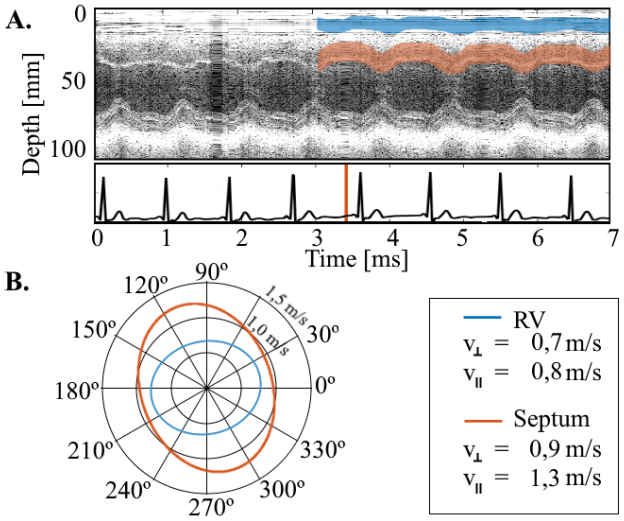

Fig. 12. In vivo Myocardial SWV estimation on a volunteer. **A.** M-Mode and ECG controller, the Right Ventricle (RV) wall is delineated in blue on the M-Mode and the septal segment in orange. **B.** The two SWV profiles and the transverse/parallel velocities are estimated from one single acquisition.

Individual and average results are presented on Table V. The average parallel SWV was 1.08m/s on the RV and 1.74 m/s on the septum. The intra patient reproducibility was +/-0.18 m/s.

TABLE V
HEALTHY VOLUNTEERS MS

Volunteer		RV		Septum
1	$v_{\parallel}$	1.08 +/- 0.08 m/s	$v_{\parallel}$	2.44 +/- 0.22 m/s
	$v_{\perp}$	0.64 +/- 0.17 m/s	$v_{\perp}$	1.82 +/- 0.08 m/s
	FA	0.35 +/- 0.17	FA	0.20 +/- 0.04
2	$v_{\parallel}$	1.06 +/- 0.17 m/s	$v_{\parallel}$	1.68 +/- 0.26 m/s
	$v_{\perp}$	0.68 +/- 0.15 m/s	$v_{\perp}$	1.34 +/- 0.29 m/s
	FA	0.31 +/- 0.06	FA	0.22 +/- 0.07
3	$v_{\parallel}$	0.94 +/- 0.25 m/s	$v_{\parallel}$	1.20 +/- 0.20 m/s
	$v_{\perp}$	0.66 +/- 0.09 m/s	$v_{\perp}$	0.86 +/- 0.11 m/s
	FA	0.22 +/- 0.14	FA	0.22 +/- 0.14
4	$v_{\parallel}$	1.24 +/- 0.20 m/s	$v_{\parallel}$	1.64 +/- 0.15 m/s
	$v_{\perp}$	0.62 +/- 0.08 m/s	$v_{\perp}$	1.10 +/- 0.12 m/s
	FA	0.44 +/- 0.04	FA	0.27 +/- 0.08
Average				
	$v_{\parallel}$	1.08 +/- 0.20 m/s	$v_{\parallel}$	1.74 +/- 0.51 m/s
	$v_{\perp}$	0.65 +/- 0.12 m/s	$v_{\perp}$	1.28 +/- 0.48 m/s
	FA	0.33+/- 0.11	FA	0.23 +/- 0.09

IV. DISCUSSION

In this study, we introduced a novel approach for quantitative assessment of myocardial stiffness. A smart ultrasound transducer was designed to achieve shear wave elastography in locally transverse isotropic soft medium. The approach was validated using numerical simulations as well as experiments in calibrated phantoms and biological samples. We demonstrated that this method is effective for assessing quantitatively the elastic properties of locally transverse isotropic soft tissues such as skeletal muscles and the myocardium without prior knowledge of the fibers' orientation. Finally, we investigated the transthoracic feasibility on the heart of 4 human volunteer and showed that this approach is feasible and reproducible with an intra-patient variability of +/- 0.18 m/s. For comparison purposes, the SWV differences between control and hypertrophic cardiomyopathy patients was reported to be larger than 2 m/s on average thus one order of magnitude larger than the measurement variability [30].

This approach was developed to provide a clinical solution to the problem of angular dependence of shear velocity estimates with respect to myocardial fiber orientations. Previous studies of 2D myocardial SWE have proposed to perform shear wave velocity estimation along standardized anatomical views. For example, Villemain et al observed in pediatric and adult patients that the shear velocities in short axis view were significantly higher than in long axis view. Assuming that fibers were mainly oriented along the circumferential direction (i.e in short axis view), the FA was estimated to 0.24 ± 0.07 in adults and of 0.14 ±0.06 in children [30]. However, such an assumption does not hold on all patients, particularly those with fiber disarray, and generally speaking, it is difficult to assume the actual fibers' orientation in human patients during echocardiography exam. Therefore, when applying 2D SWE imaging, the shear velocity is estimated in an unknown direction with respect to the fibers' orientation. The discrepancy between parallel and transverse velocity may induce high variability among patient measurements and creates a certain ambiguity of which stiffness is really measured (along/across the fibers).

Other approaches for myocardial stiffness evaluation have relied on shear waves induced by physiological events such as valve closures (mitral or aortic valves [4]), blood pressure waves (atrial kick [5]) or even by contraction propagation (electromechanical coupling [6]). Methods based on natural shear waves were shown to be feasible in vivo [7] and were recently applied to Amyloidosis patients [8] with promising results. However, these approaches do not solve the problem of tissue anisotropy. Moreover, relying on natural shear waves has additional limitations: the generation of natural waves in the myocardium is a complex tri-dimensional phenomenon and is challenging to assess using 2D imaging [9], the wavelength of these natural waves is very large ~10cm which makes the wave velocity strongly dependent on myocardial anatomy and wall thickness. Moreover, the shear wave source is uncontrolled in terms of location, wavelength, amplitude and timing during the cardiac cycle [9]. 3D UF approaches have been proposed [32] – [35] to image the tri-dimensional wave propagation but in these studies the quantification of the velocity remains challenging. Moreover, none of these approaches could assess the elastic anisotropy of the myocardium.

In contrast, our approach is based on a well-controlled source location and timing using the acoustic radiation force. Thanks to the sharp shear source generated at a well-defined location in the myocardium, the resulting velocity profile can be quantified accurately in several directions simultaneously. We therefore achieved a 3D segmental estimation using a simple transducer design without the complexity of a full 3D UF device. This design offers reliable and robust shear velocity estimate.

We designed intentionally a low complexity 8-element ultrasound device in order to ease as much as possible the clinical translational and dissemination. The system presented in this study could be entirely controlled by electronics with only 8-channels which is much more affordable in term of cost and complexity that high channel count electronics used in 2D or 3D UF imaging.

This new approach could have several important applications in cardiology. Non-invasive stiffness assessment of the myocardium could become a major biomarker of diastolic dysfunction which remains difficult to quantify accurately with current clinical imaging tools. Myocardial stiffness could be applied to the diagnostic of heart failure with preserved ejection fraction, cardiomyopathies or cardiac amyloidosis, all of which remain difficult to diagnose. Non-invasive myocardial stiffness assessment could be also important for the diagnosis and prognosis of heart transplant recipient as proposed by Petrescu et al. [37]

Nevertheless, our approach should be envisioned mostly for the diagnostic of diffuse or global heart impairments because of the limited number of myocardial segments that can be reached. The right ventricular free wall and the septal wall can be assessed from the parasternal view as shown in this study whereas the septal wall and apical segment could be reached from the apical view. The left ventricular posterior wall, however, was not accessible because of the depth limitation of the current transducer. The regional stiffness assessment could also be interesting in some specific pathologies with myocardial

heterogeneity. In these situations, the regional function is not always linked to the global function and the regional stiffness could bring new clinical information.

In this study, we limited the acquisition of the myocardial stiffness on the human volunteer to the mid-diastolic phase. However, the acquisition can be performed at any time of the cardiac cycle for to real time evaluation of myocardial elastic properties. SWV variation over the entire cardiac cycle could provide new insight of the cardiac function. Limitations of the study include the assumption of a purely elastic anisotropic material in Eq.2. The shear wave propagation model could be complexified in further study in order to include the viscosity properties. The lack of analytical solutions may however complicate the derivation of the visco-elastic properties.

A limitation of the approach is the need to estimate simultaneously three times of flight to achieve the inversion. For any reason, if one of the three estimates are missing, the inversion cannot be computed. A large number of acquisitions can be performed to minimize this risk. Another potential solution would be to add several lateral elements in additional directions. It would allow to do measurement even if one element are missing but it would require to revise the transducer geometry.

Another limitation of the approach is the positioning of the probe based on real-time M-mode imaging without 2D imaging modality. As it is not a standard procedure for cardiologists, it may require a special training to achieve the positioning. Nevertheless, the learning curve was smooth for the cardiologist of the study who was rapidly able to position the transducer without the need of 2D imaging. The entire procedure including positioning and shear wave acquisitions took about 1-2 minutes. A solution to improve the positioning would be to integrate a two-dimensional phased array into the transducer.

V. CONCLUSION

In this study, we introduced a novel approach for non-invasive real-time quantification of transverse isotropic elastic properties. A smart ultrasound device with a small number of transducer elements was developed to measure simultaneously the SWV in three directions and provide the parallel and transverse SWV. We validated the approach using numerical simulations and experiments in calibrated phantoms and ex vivo tissue samples. Finally, we demonstrated the transthoracic feasibility and reproducibility in the human beating heart. The smart ultrasound device has therefore the potential to become a portable and highly disseminable clinical tool for the assessment of myocardial stiffness and function.

Bibliography

[1] "ESC Guidelines for the diagnosis and treatment of acute and chronic heart failure 2012: The Task Force for the Diagnosis and Treatment of Acute and Chronic Heart Failure 2012 of the European Society of Cardiology. Developed in collaboration with the Heart Failure Association (HFA) of the ESC - PubMed." https://pubmed.ncbi.nlm.nih.gov/22611136/

[2] "Myocardial Stiffness in Patients With Heart Failure and a Preserved Ejection Fraction | Circulation." https://www.ahajournals.org/doi/10.1161/CIRCULATIONAHA.114.013215?url_ver=Z39.88-2003&rfr_id=ori:rid:crossref.org&rfr_dat=cr_pub%20%200pubmed

[3] M. R. Zile, C. F. Baicu, and W. H. Gaasch, "Diastolic Heart Failure — Abnormalities in Active Relaxation and Passive Stiffness of the Left Ventricle," *http://dx.doi.org/10.1056/NEJMoa032566*, Oct. 08, 2009. https://www.nejm.org/doi/10.1056/NEJMoa032566

[4] G. P. Aurigemma, M. R. Zile, and W. H. Gaasch, "Lack of relationship between Doppler indices of diastolic function and left ventricular pressure transients in patients with definite diastolic heart failure," *Am. Heart J.*, vol. 148, no. 3, p. E12, Sep. 2004, doi: 10.1016/j.ahj.2004.01.022.

[5] J. Bercoff, M. Tanter, and M. Fink, "Supersonic shear imaging: a new technique for soft tissue elasticity mapping," *IEEE Trans Ultrason Ferroelectr Freq Control*, vol. 51, no. 4, pp. 396–409, Apr. 2004.

[6] M. Pernot, M. Couade, P. Mateo, B. Crozatier, R. Fischmeister, and M. Tanter, "Real-time assessment of myocardial contractility using shear wave imaging," *J. Am. Coll. Cardiol.*, vol. 58, no. 1, pp. 65–72, Jun. 2011, doi: 10.1016/j.jacc.2011.02.042.

[7] M. Pernot *et al.*, "Shear Wave Imaging of Passive Diastolic Myocardial Stiffness: Stunned Versus Infarcted Myocardium," *JACC Cardiovasc Imaging*, vol. 9, no. 9, pp. 1023–1030, 2016, doi: 10.1016/j.jcmg.2016.01.022.

[8] M. Vejdani-Jahromi, J. Freedman, M. Nagle, Y.-J. Kim, G. Trahey, and P. Wolf, "Quantifying Myocardial Contractility Changes Using Ultrasound-Based Shear Wave Elastography," *Journal of the American Society of Echocardiography : official publication of the American Society of Echocardiography*, 2017, doi: 10.1016/j.echo.2016.10.004.

[9] M. Couade *et al.*, "In vivo quantitative mapping of myocardial stiffening and transmural anisotropy during the cardiac cycle," *IEEE Trans Med Imaging*, vol. 30, no. 2, pp. 295–305, Feb. 2011, doi: 10.1109/TMI.2010.2076829.

[10] M. Pernot, M. Couade, P. Mateo, B. Crozatier, R. Fischmeister, and M. Tanter, "Real-time assessment of myocardial contractility using shear wave imaging," *J. Am. Coll. Cardiol.*, vol. 58, no. 1, pp. 65–72, Jun. 2011, doi: 10.1016/j.jacc.2011.02.042.

[11] M. Pernot *et al.*, "Shear Wave Imaging of Passive Diastolic Myocardial Stiffness: Stunned Versus Infarcted Myocardium," *JACC Cardiovasc Imaging*, vol. 9, no. 9, pp. 1023–1030, 2016, doi: 10.1016/j.jcmg.2016.01.022.

[12] P. Song *et al.*, "Quantitative Assessment of Left Ventricular Diastolic Stiffness Using Cardiac Shear Wave Elastography: A Pilot Study.," *Journal of ultrasound in medicine : official journal of the American Institute of Ultrasound in Medicine*, 2016, doi: 10.7863/ultra.15.08053.

[13] M. Correia, J. Provost, S. Chatelin, O. Villemain, M. Tanter, and M. Pernot, "Ultrafast Harmonic Coherent Compound (UHCC) Imaging for High Frame Rate

Echocardiography and Shear-Wave Elastography," *IEEE Trans Ultrason Ferroelectr Freq Control*, vol. 63, no. 3, pp. 420–431, Mar. 2016, doi: 10.1109/TUFFC.2016.2530408.

[14] O. Villemain *et al.*, "Myocardial Stiffness Evaluation Using Noninvasive Shear Wave Imaging in Healthy and Hypertrophic Cardiomyopathic Adults," *JACC Cardiovasc Imaging*, Mar. 2018, doi: 10.1016/j.jcmg.2018.02.002.

[15] W.-N. Lee *et al.*, "Mapping myocardial fiber orientation using echocardiography-based shear wave imaging," *IEEE Trans Med Imaging*, vol. 31, no. 3, pp. 554–562, Mar. 2012, doi: 10.1109/TMI.2011.2172690.

[16] Y. C. Fung, *Biomechanics: Mechanical Properties of Living Tissues*, 2nd ed. New York: Springer-Verlag, 1993.

[17] J. Brum, M. Bernal, J. L. Gennisson, and M. Tanter, "In vivoevaluation of the elastic anisotropy of the human Achilles tendon using shear wave dispersion analysis," *Phys. Med. Biol.*, vol. 59, no. 3, pp. 505–523, Jan. 2014, doi: 10.1088/0031-9155/59/3/505.

[18] H. Kanai, "Propagation of spontaneously actuated pulsive vibration in human heart wall and in vivo viscoelasticity estimation," *IEEE Transactions on Ultrasonics, Ferroelectrics, and Frequency Control*, vol. 52, no. 11, pp. 1931–1942, Nov. 2005, doi: 10.1109/TUFFC.2005.1561662.

[19] W.-N. Lee, B. Larrat, M. Pernot, and M. Tanter, "Ultrasound elastic tensor imaging: comparison with MR diffusion tensor imaging in the myocardium," *Phys Med Biol*, vol. 57, no. 16, pp. 5075–5095, Aug. 2012, doi: 10.1088/0031-9155/57/16/5075.

[20] J.-L. Gennisson *et al.*, "4-D ultrafast shear-wave imaging," *IEEE Transactions on Ultrasonics, Ferroelectrics, and Frequency Control*, vol. 62, no. 6, pp. 1059–1065, Jun. 2015, doi: 10.1109/TUFFC.2014.006936.

[21] M. Correia, T. Deffieux, S. Chatelin, J. Provost, M. Tanter, and M. Pernot, "3D elastic tensor imaging in weakly transversely isotropic soft tissues," *Phys. Med. Biol.*, vol. 63, no. 15, p. 155005, Jul. 2018, doi: 10.1088/1361-6560/aacfaf.

[22] D. ROYER and E. Dieulesaint, *Elastic Waves in Solids I: Free and Guided Propagation*. Berlin Heidelberg: Springer-Verlag, 2000.

[23] J. A. Jensen, "A model for the propagation and scattering of ultrasound in tissue," *The Journal of the Acoustical Society of America*, vol. 89, no. 1, pp. 182–190, Jan. 1991, doi: 10.1121/1.400497.

[24] J. A. Jensen and N. B. Svendsen, "Calculation of pressure fields from arbitrarily shaped, apodized, and excited ultrasound transducers," *IEEE Trans. Ultrason., Ferroelect., Freq. Contr.*, vol. 39, no. 2, pp. 262–267, Mar. 1992, doi: 10.1109/58.139123.

[25] V. Vavryčuk, "On the retrieval of moment tensors from borehole data," *Geophysical Prospecting*, vol. 55, no. 3, pp. 381–391, 2007, doi: 10.1111/j.1365-2478.2007.00624.x.

[26] S. Chatelin, J.-L. Gennisson, M. Bernal, M. Tanter, and M. Pernot, "Modelling the impulse diffraction field of shear waves in transverse isotropic viscoelastic medium," *Phys. Med. Biol.*, vol. 60, no. 9, pp. 3639–3654, May 2015, doi: 10.1088/0031-9155/60/9/3639.

[27] C. Kasai, K. Namekawa, A. Koyano, and R. Omoto, "Real-Time Two-Dimensional Blood Flow Imaging Using an Autocorrelation Technique," p. 7.

[28] M. Palmeri, M. Wang, J. Dahl, K. Frinkley, and K. Nightingale, "Quantifying hepatic shear modulus in vivo using acoustic radiation force.," *Ultrasound in medicine & biology*, 2008, doi: 10.1016/j.ultrasmedbio.2007.10.009.

[29] M. Wang, B. Byram, M. Palmeri, N. Rouze, and K. Nightingale, "Imaging Transverse Isotropic Properties of Muscle by Monitoring Acoustic Radiation Force Induced Shear Waves using a 2D Matrix Ultrasound Array," *IEEE Trans Med Imaging*, vol. 32, no. 9, pp. 1671–1684, Sep. 2013, doi: 10.1109/TMI.2013.2262948.

[30] O. Villemain *et al.*, "Myocardial Stiffness Evaluation Using Noninvasive Shear Wave Imaging in Healthy and Hypertrophic Cardiomyopathic Adults," *J Am Coll Cardiol Img*, vol. 12, no. 7 Part 1, pp. 1135–1145, Jul. 2019, doi: 10.1016/j.jcmg.2018.02.002.

[31] M. Couade *et al.*, "In Vivo Quantitative Mapping of Myocardial Stiffening and Transmural Anisotropy During the Cardiac Cycle," *IEEE Transactions on Medical Imaging*, 2011, doi: 10.1109/TMI.2010.2076829.

[32] C. Papadacci *et al.*, "4D simultaneous tissue and blood flow Doppler imaging: revisiting cardiac Doppler index with single heart beat 4D ultrafast echocardiography," *Phys Med Biol*, vol. 64, no. 8, p. 085013, 10 2019, doi: 10.1088/1361-6560/ab1107.

[33] M. Correia, J. Provost, M. Tanter, and M. Pernot, "4D ultrafast ultrasound flow imaging: in vivo quantification of arterial volumetric flow rate in a single heartbeat," *Phys Med Biol*, vol. 61, no. 23, pp. L48–L61, 07 2016, doi: 10.1088/0031-9155/61/23/L48.

[34] C. Papadacci, V. Finel, O. Villemain, M. Tanter, and M. Pernot, "4D ultrafast ultrasound imaging of naturally occurring shear waves in the human heart," *IEEE Transactions on Medical Imaging*, pp. 1–1, 2020, doi: 10.1109/TMI.2020.3020147.

[35] S. Salles *et al.*, "3D Myocardial Mechanical Wave Measurements: Toward In Vivo 3D Myocardial Elasticity Mapping," *J Am Coll Cardiol Img*, Aug. 2020, doi: 10.1016/j.jcmg.2020.05.037.

[36] O. Villemain *et al.*, "Myocardial Stiffness Evaluation Using Noninvasive Shear Wave Imaging in Healthy and Hypertrophic Cardiomyopathic Adults," *JACC. Cardiovascular imaging*, 2018, doi: 10.1016/j.jcmg.2018.02.002.

[37] A. M. Petrescu *et al.*, "P2476Non-invasive left ventricular stiffness measurements for assessing diastolic myocardial properties after orthotopic heart transplantation," *Eur Heart J*, vol. 40, no. Supplement_1, Oct. 2019, doi: 10.1093/eurheartj/ehz748.0807.